

Carlos M. García · Marcelo H. García

Characterization of flow turbulence in large-scale bubble-plume experiments

Received: 18 December 2005 / Revised: 25 March 2006 / Accepted: 21 April 2006 / Published online: 30 May 2006
© Springer-Verlag 2006

Abstract Flow turbulence generated by a bubble plume in a large tank is characterized. Two different turbulence mechanisms contributing to the mixing and transport process are identified on velocity signals recorded outside of the bubble-plume core: a macro-scale process governed by the wandering motion of the bubble-plume; and an intermediate- and micro-scale process represented by the Kolmogorov power spectrum. A methodology is presented to characterize the different processes and their contributions to the turbulence parameters. The results help to understand the bubble-plume phenomenon and provide a basis to validate numerical models of bubble-plumes used in the design of combined-sewer-overflow reservoirs.

1 Introduction

Bubble-plumes are commonly used to generate circulation and mixing in a liquid body. An aeration system consisting of coarse bubble diffusers is expected to be used in combined-sewer-overflow (CSO) reservoirs that are being built by the Metropolitan Water Reclamation District of Greater Chicago (MWRDGC) as part of the tunnel and reservoir plan (TARP). Those reservoirs will help to reduce flood damage and minimize releases of untreated sewage to the waterways in the Chicago Metropolitan area. The U.S. Army Corps of Engineers (Chicago District) provided researchers at the University of Illinois at Urbana-Champaign (UIUC) the funding necessary to perform a set of water-velocity measure-

ments in a large-scale bubble-plume facility under non-stratified conditions (Fig. 1). The analysis of the recorded data sets provides a wealth of information for the modeling and design of a full-scale aeration system for McCook Reservoir (storage $\approx 3 \times 10^7 \text{ m}^3$), one of the CSO reservoirs to be built as part of TARP project in Chicago. Both the flow turbulence and the flow dynamics generated by the bubble-plumes must be well characterized to obtain an accurate quantification of the induced mixing and associated transport processes in the reservoir.

Experimental observations of medium and large-scale bubble-plumes in non-stratified conditions (water depths varying between 1 and 60 m) were performed by Baines and Hamilton (1959), Kobus (1968), Tekeli and Maxwell (1978), Milgram (1983), Johnson et al. (2000), Soga and Rehmann (2004), and Wain and Rehmann (2005). Most of these studies have focused on the experimental description of the mean velocity profiles, recirculation patterns, bubble characterization and entrainment of ambient fluid into the plume. Only a few of the cited experimental observations of bubble-plumes have characterized turbulence parameters. Tekeli and Maxwell (1978) were among the first to report values of turbulent intensities in a medium-scale, bubble-plume facility. Soga and Rehmann (2004) and Wain and Rehmann (2005) computed vertical profiles of dissipation rate of turbulent kinetic energy and eddy viscosity, respectively, using a self-contained autonomous microprofiler (SCAMP) in the same facility used for the work described herein, but only low-air discharge conditions were characterized because of limitations in the range of application of SCAMP (Kocsis et al. 1999).

It is well known that a bubble plume often presents a wandering motion (Baines and Hamilton 1959; Fannelop et al. 1991; Fischer et al. 1994; Mudde et al. 1997b; Becker et al. 1999; Rensen and Roig 2001; Buwa and Ranade 2002; Joshi et al. 2002; Mudde 2005). The large-amplitude wandering is a macro-scale turbulent process caused by the effects of the tank walls when the horizontal extent of the facility is not large in comparison

C. M. García (✉) · M. H. García
Ven T. Chow Hydrosystems Laboratory,
Department of Civil and Environmental Engineering,
University of Illinois at Urbana-Champaign,
205 North Mathews Ave., Urbana, IL 61801, USA
E-mail: cgarcia2@uiuc.edu
Tel.: +1-217-3336183
Fax: +1-217-3330687

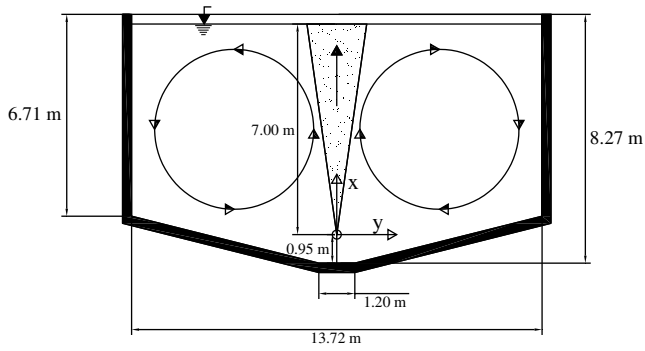


Fig. 1 Cross-section view of the digester tank (x , y and z are vertical, radial, and tangential coordinates)

with the plume diameter (Milgram 1983; Fannelop et al. 1991). An intermediate- and micro-scale turbulence process, with an energy distribution well represented by a Kolmogorov power spectrum, is superimposed on the wandering macro-scale turbulence process. These two processes produce turbulence at very different scales, thus contributing in different ways to the mixing in the tank. A methodology is presented herein to characterize the different scale associated with the turbulence generated by a bubble plume in a large tank and their contributions to the turbulence parameters. Results of applying the methodology to water-velocity signals recorded at a defined location in the tank are presented and used to evaluate the behavior of some turbulence parameters (wandering frequency of the bubble plume, turbulent kinetic energy TKE, turbulence time and length scales, and dissipation rate of TKE) as the air discharge varies.

2 Experimental set-up

Experiments were conducted in a large-scale bubble-plume facility built on a digester tank owned by the Urbana and Champaign Sanitary District (UCSD) located at the UCSD Northeast Wastewater Treatment Plant in Urbana, IL, USA (Fig. 1). A 0.61 m long stainless-steel coarse-bubble diffuser, typically used in aeration tanks, sludge holding tanks, and aerobic digesters, was located at 0.95 m above the bottom in the center of the tank.

Fig. 2 a Coarse-bubble diffuser located 0.95 m above the bottom in the center of the tank. **b** Down rod with six acoustic Doppler velocimeter probes arranged vertically at different distances above the diffuser

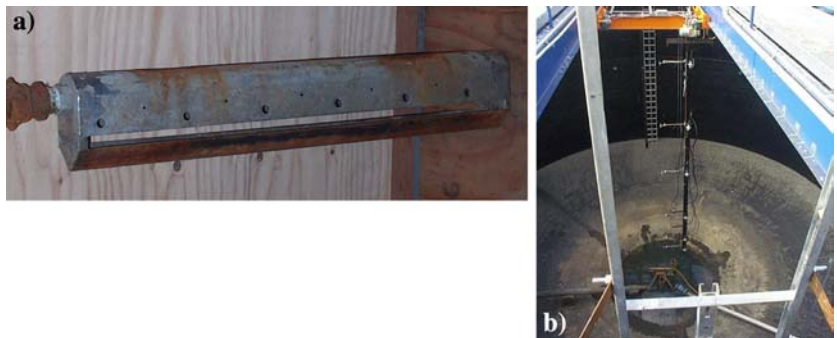


Figure 2a shows the coarse-bubble diffuser used in the experiments, which is manufactured by Aercor in Worcester, Massachusetts. The same diffuser was used previously in a related study by Johnson et al. (2000) in coarse-bubble diffuser tests. At low-flow rates, the compressed air escaped from twelve 5 mm circular openings and twelve 10 mm circular openings. At higher flow rates the compressed air was also released from two 10 mm lateral slots that run the length of the diffuser on both sides. Air-flow rates were monitored using flow meters manufactured by Meter Equipment Manufacturing. A pressure-regulating valve was included between the compressor and the flow meters to insure a constant airflow rate to the diffuser.

The tank was filled to a water depth of 7 m above the diffuser for all experiments. Six different experimental conditions are analyzed in this paper. The volumetric air discharge at atmospheric pressure (Q_g), the water temperature (T) and a description of the quality of the water (WQ) used to fill the tank for each test are given in Table 1.

3 Measurement devices

Six 10 MHz Nortech NDVField acoustic Doppler velocimeter probes (sampling volume with a diameter of 6 mm is located 10 cm from the tip of the probe) were placed on a down-looking, steel rod and arranged vertically at different distances above the diffuser (Fig. 2b). A side-looking orientation for the instruments was used in all the measurements.

The capacity of the acoustic Doppler velocimetry (ADV) technique to accurately resolve flow turbulence was evaluated by García et al. (2005a). The ADV technique produces a reduction of all the even moments in the water-velocity signal because of the sampling strategy used by this technique. This sampling strategy also affects the computed autocorrelation function, the time scales derived from them (which turnout to be high biased), and the power spectrum (less resolution of the inertial range). García et al. (2005a) claimed that all these effects are negligible in cases where a value of the dimensionless frequency, $F = f_R L / U_c$, higher than 20 is used, where f_R is the user defined sampling frequency, L is the energy-containing eddy length scale, and U_c is the

Table 1 Experimental conditions for each analyzed test

Test	Q_g (L/s)	T (°C)	WQ	BOD (mg/L)	TSS (mg/L)
5	16.52	15.5	NP	–	–
6	5.43	16.0	NP	–	–
7	0.61	15.5	NP	–	–
11	0.19	25.1	SE	36	58
13	10.85	24.5	SE	96	160
15	3.30	13.9	SE	96	160

NP non-potable influent, *SE* sewage influent, *BOD* biochemical oxygen demand, *TSS* total suspended solid

convective velocity of the flow at the measurement point. The ratio U_c/f_R defines the diameter of the spatial sampling interval (d_R) set by the flow and sampling characteristics of the ADV. The diameter d of the ADV sampling volume defined by the beam geometry is used in the computation of F instead of d_R when the value of d_R is smaller than the diameter d (smallest air discharges). Representative values of convective velocity and energy-containing eddy length-scale for water-velocity signals recorded in the tank outside of the bubble core were in the order of 0.10 m/s and 1 m, respectively. Thus, even for $f_R = 10$ Hz, F was always higher than 20 which proved that the ADV technique was able to report a good description of the turbulence for the flow conditions analyzed in this paper. Velocity measurements began at least 1 h after the air started flowing to reach steady conditions in the tank. A value of f_R equal to 25 Hz was used in tests 5, 6, and 7, whereas a value of f_R equal to 10 Hz was used in tests 11, 13, and 15 to reduce the noise energy levels of the recorded signals. Due to the wandering motion of the bubble plume, only time averaged measurements over a long period of time give reliable results (Baines and Hamilton 1959; Kobus 1968; Johansen et al. 1988; Fannelop et al. 1991; Becker et al. 1994). Water-velocity time series were recorded simultaneously by the six sensors during a period of 20 min at each radial location (0.00, 0.15, 0.30, 0.46, 0.61, 0.76, 0.91, 1.07, 1.22, 1.37, 1.52, 1.83, 2.13, 2.59, 3.05, 3.96, and 4.88 m from the center of the tank). Representative flow-turbulence statistics could not be computed from time series recorded at radial locations inside of the bubble core because of the limitations of ADV technique to measure where bubbles are present, however these signals helped in the characterization of the plume wandering motion.

4 Estimation of the plume wandering frequency

Wandering motion of the bubble plume was detected for all the analyzed experimental conditions. The presence of plume wandering is manifested on the velocity signals recorded inside of the bubble core. The passage of bubbles on the sampling volume of each velocity sensor generated a noise behavior in the signal and the presence of the bubbles on the sampling volume was intermittent because of the wandering motion of the bubble-plume.

Figure 3 shows five 20-min-long vertical velocity signals recorded during test 5 using five ADV sensors simultaneously set at different vertical locations above the diffuser (5.3, 3.9, 2.4, 1.5, and 1.0 m) at a radial distance of 0.46 m from the vertical axis of the plume (inside the bubble-plume core). The energy of the signals recorded inside of the bubble-plume core was overestimated because of the presence of bubble bursts but estimates of the wandering frequency of the plume were computed detecting the frequency where the peak was observed in the energy power spectra of each recorded velocity signal. The analysis was expanded to signals recorded at ten radial locations (≤ 1.37 m from the axis) where the intermittent presence of bubbles was observed. The analysis includes only signals recorded at a single vertical location (3.9 m above the diffuser) because simultaneously recorded signals (other vertical locations) did not provide independent estimates. For test 5, the more frequent (mode) wandering period (T_s) observed at the ten radial locations was $T_s = 328$ s.

Estimates of T_s were computed using the same approach for flow conditions generated by different air discharges (Q_g). Values of T_s as a function of Q_g , are shown in Fig. 4. The error bars in Fig. 4 represent the estimated uncertainty in detecting the peak frequency in the power spectra of each recorded velocity signal. The uncertainty in T_s decreased from ± 50 to $\pm 25\%$ as the air discharge increase from 3.30 to 16.52 L/s. Wandering periods for the two smallest air-discharge values (air discharge 0.19 and 0.61 L/s) could not be accurately defined experimentally based in 20-min-long, water-velocity signals.

The same behavior of T_s was found for the vertical and radial velocity component signals recorded inside of the bubble core and the mode frequencies were 67, 75, 78, and 80% for the vertical velocity component and 44, 63, 67, and 80% for the radial velocity component for air discharges of 3.30, 5.43, 10.85, and 16.52 L/s, respectively. The trend observed in Fig. 4 agrees with observations in bubble columns by Fischer et al. (1994),

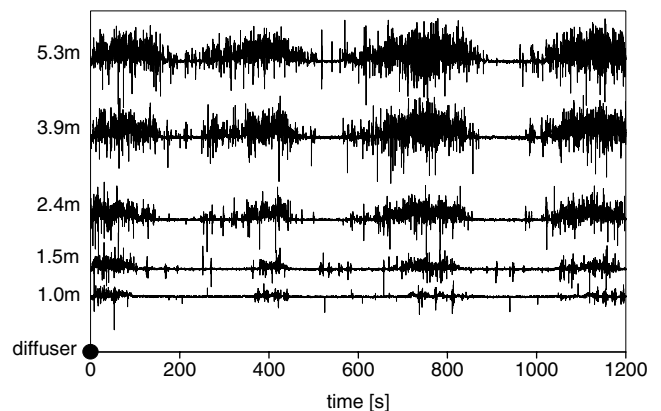


Fig. 3 Vertical water-velocity signals recorded during test 5 at radial location = 0.46 m and vertical positions 1.0, 1.5, 2.4, 3.9, and 5.3 m above the diffuser

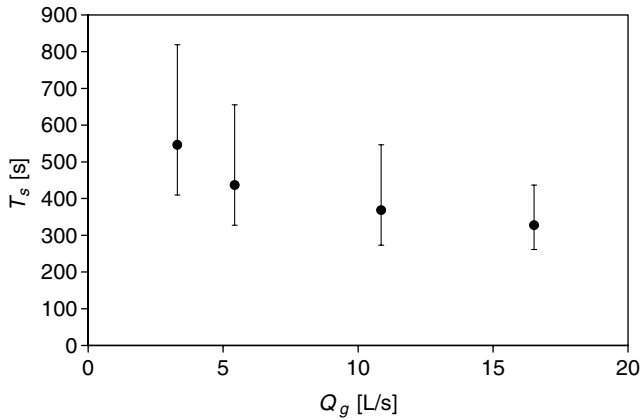


Fig. 4 More frequent (mode) wandering period of the bubble plume observed for different air discharges

Mudde et al. (1997a), Rensen and Roig (2001), and Buwa and Ranade (2002), in that the wandering period of the plume decreased as the air discharge increased. Delnoij et al. (1997) and Rensen and Roig (2001) observed that for tanks with aspect ratio higher than 3, defined by the ratio between water depth and tank diameter, the frequency of the oscillation of the water-velocity signals does not depend on the aspect ratio, but for smaller values of the aspect ratio the frequency decreases as the aspect ratio does. For that reason the values of wandering frequency observed for an aspect ratio lower than 3 (some as the tank in this work) can not be directly compared with the available values observed in bubble columns which usually have an aspect ratio higher than 3.

The effects of the wandering motion are not restricted only to velocity signals recorded inside of the bubble core. The plume wandering generated a random low-frequency periodic component in velocity signals recorded at the entire tank. The observed wandering periods in the entire tank were of the same order as the values computed inside of the bubble-core describing the observed plume structure in time. This result agrees with observations cited by Becker et al. (1999) and Buwa and Ranade (2002). However, the behavior is more irregular and the frequency of the period mode is smaller outside of the bubble core. Figure 5 shows the low-frequency component (thick line) in the water-velocity signal recorded at a defined location outside of the bubble core (3.05 m from the central axis of the tank, vertical location 5.3 m above the diffuser).

5 Proposed signal-processing technique

The presence of three different random processes in the recorded velocity signals is evident in the computed power spectrum (G_{yy} in Fig. 6) for the radial velocity signal showed in Fig. 5. The power spectrum (Fig. 6) was computed through the fast Fourier transform (FFT) of the windowed data (a rectangular window was used). The

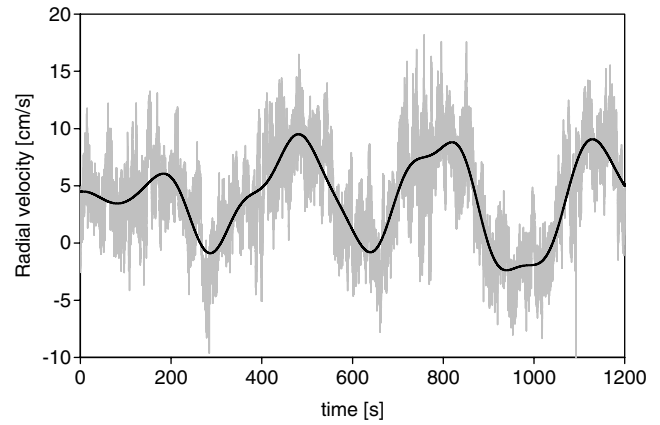


Fig. 5 Gray line is the radial water-velocity signal recorded at 3.05 m from the axis of the tank, vertical location 5.3 m above the diffuser (test 5). The black line is the low-frequency component of the signal obtained using a low-pass filter with a cutoff frequency of (1/120) Hz

number of segments (Bendat and Piersol 2000) selected to get the average power spectrum reported in Fig. 6 was minimized to represent all the turbulence processes present in the tank (including the low frequency ones) with the cost of higher uncertainty in the reported values of the power spectra. The macro-scale turbulence process (wandering) is observed in Fig. 6 through a peak at the low-frequency component of the spectrum. Then, the intermediate- and micro-scale turbulence process is well represented by a typical Kolmogorov power spectrum and, finally, the presence of noise intrinsic to the selected measurement technique (Doppler technique) is visualized as a flat plateau at the high frequency range. The area below the power spectrum is the energy of the recorded radial velocity signal at this location. Based on the hypothesis that fluctuations contributions from the

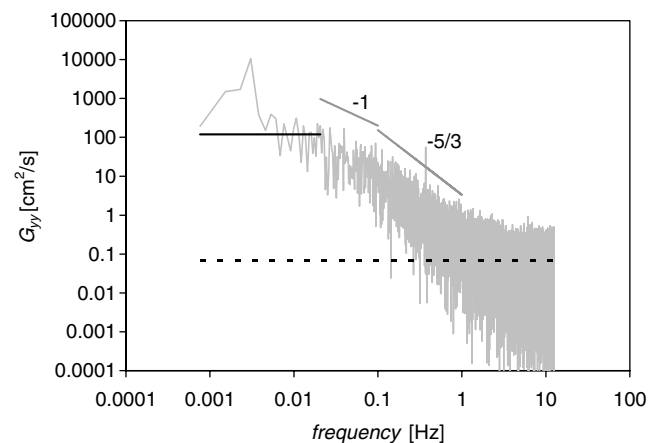


Fig. 6 One-dimensional power spectrum in the frequency domain (G_{yy}) for the recorded radial water-velocity signal represented in Fig. 5. Dashed line indicates noise energy level. Solid line indicates energy level of the low-frequency component of the intermediate- and micro-scale turbulence process. $-5/3$ and -1 slopes are also indicated

macro-, intermediate- and micro-scale turbulence processes and noise are uncorrelated, the total recorded spectrum is composed by the sum of the spectrum generated for each of these random processes. Following, a signal-processing technique is proposed to remove the noise energy component from the recorded power spectrum and to separately characterize the two observed different scale turbulence process.

5.1 Removing noise contributions

The main source of error in the acoustic Doppler velocimetry technique is the Doppler noise. The Doppler noise has the characteristics of white noise (Nikora and Goring 1998) with a flat power spectrum that indicates the presence of uncorrelated noise. Because of these characteristics, the Doppler noise cannot be removed from the recorded signal using filtering techniques; however, corrections to the turbulence parameters (turbulent kinetic energy, length and time scales, convective velocity, and dissipation rate of turbulent kinetic energy) were performed after the noise energy level of the signal was detected. In low-energy flow, the energy level of the white noise can be identified in a power spectrum as a flat plateau at high frequencies (see Fig. 6). Empirical spectra of the Doppler noise were replaced by straight horizontal lines (Nikora and Goring 1998) where the ordinates are equal to the average noise energy level (NEL) for frequencies within the highest 1 Hz range in the recorded power spectra (Voulgaris and Trowbridge 1998). In cases of very high energy flow, (test 5, $Q_g = 16.52$ L/s; and test 13, $Q_g = 10.85$ L/s) or very small noise energy level (test 15, $Q_g = 3.30$ L/s), this method can not be used because the noise energy level is not detected in the spectrum at high frequencies. García et al. (2005a) proved that the noise energy in these tests is smaller than 10% of the real total energy. For velocity signals recorded during tests 5, 13, and 15, an upper limit for a noise energy level was computed using the observed energy value from the spectrum at the Nyquist frequency (half of the recording frequency) assuming that the flat plateau would be detected in the spectrum just after the Nyquist frequency. Details of the proposed technique to correct the different turbulence parameters using the detected noise energy levels are included in Sect. 6 at the time the methodology used to compute each turbulence parameter is described. Noise corrections were not performed to the mean and shear-stress parameters because the Doppler noise does not affect them (Nikora and Goring 1998; Voulgaris and Trowbridge 1998).

5.2 Separating different scale turbulence process

Time scales (period) of the macro-scale turbulence process produced by the plume wandering defined before (of the order of 300 s, see Fig. 4), were about

two orders of magnitude longer than the integral time scale of the intermediate- and micro-scale turbulence process. This result allows the use of separation techniques to obtain information characterizing each turbulence-generating mechanism. The simplest available technique consists on averaging the velocity data at constant phase of a periodic signal but this technique did not work here because the macro-scale turbulence process is not monochromatic (the period of the wandering motion is a random variable). The selected separation technique consists of high pass filtering the recorded water-velocity signal (Fig. 5). The high pass filtering was performed using a FFT (rectangular window), making zero all Fourier components for frequencies lower than the cut-off filter frequency and then applying the inverse FFT to obtain the filtered signal. A fixed cut-off frequency value f_c equal to (1/120) Hz was defined for the entire tank and for all the air discharges. The selected cut-off frequency was selected to be higher than the highest observed wandering frequencies in the signal (see Fig. 4) but small enough to avoid significantly affecting the energy of the intermediate- and micro-scale turbulence components of the signal. After the two different turbulence processes were separated, the turbulence parameters were computed based on data characterizing each process and contributions of each process to the total values of each turbulence parameter (i.e. TKE) were assessed.

6 Methodology used to compute the turbulence parameters

6.1 Turbulent kinetic energy

The turbulent kinetic energy TKE was computed as $TKE = 1/2(u'^2 + v'^2 + w'^2)^{0.5}$, where u'^2 , v'^2 , and w'^2 indicate the variance of the signals $u(t)$, $v(t)$ and $w(t)$ characterizing the different turbulence mechanisms for the vertical, radial, and tangential velocity components, respectively. Because the measured energy using acoustic Doppler velocimeters is biased high due to Doppler noise (Lohrmann et al. 1994), the variances involved in the computation were corrected. The noise contributions were removed first from the power spectrum of each recorded water-velocity component signal using the energy noise-level defined before, simply subtracting this level from the measured spectra. Then, the corrected variance of the analyzed signal was computed as the area below the corrected power spectrum in the frequency domain.

6.2 Convective velocity

Convective velocities for the vertical, radial, and tangential directions were estimated following Heskestad

(1965). For the convective velocity in the vertical direction U_c the estimate is

$$U_c^2 = U^2 \left[1 + 2 \frac{V^2}{U^2} + 2 \frac{W^2}{U^2} + \frac{u^2}{U^2} + 2 \frac{v^2}{U^2} + 2 \frac{w^2}{U^2} \right], \quad (1)$$

where U , V , and W are the mean velocities in the vertical, radial, and tangential directions, respectively. Corrected values of the variances due to noise presence were used to obtain corrected values of the convective velocity. Equation 1 has been commonly used to compute convective velocity in flows that present large turbulence intensities such as turbine agitated tanks (Wu and Patterson 1989; Kresta and Wood 1993; Wernersson and Trägårdh 2000).

6.3 Turbulence flow scales

The integral time scale T characterizing the larger flow turbulent structures was computed integrating, to the first zero crossing, the autocorrelation function in the time domain (Kresta and Wood 1993; Wernersson and Trägårdh 2000). For the vertical direction x

$$T_x = \int_0^{t_0} R_{xx}(\tau) \cdot d\tau, \quad (2)$$

where $R_{xx}(\tau)$ is the autocorrelation function defined as $R_{xx}(\tau) = \langle (u(t) - U)(u(t + \tau) - U) \rangle$, and t_0 is the first zero crossing lag time. The autocorrelation function was estimated here through the inverse FFT of the power spectrum corrected because of the presence of the Doppler noise. The integral length scale was computed using the convective velocity value (i.e. for the vertical direction x , $L_x = T_x U_c$). Wu and Patterson (1989) suggested the use of a resultant integral length scale that takes into account the three dimensionality and anisotropy of the flow given as $L = (L_x^2 + L_y^2 + L_z^2)^{1/2}$. Finally, the order of magnitude of the smallest scale of turbulent motion (Kolmogorov length scale) is estimated using a scaling analysis as $\eta \approx (\nu^3/\varepsilon)^{1/4}$, where ν is the kinematic viscosity of the water and ε is the dissipation rate of turbulent kinetic energy (Pope 2000). The spatial resolution obtained from the selected measurement technique precluded the estimation of the Kolmogorov length scale directly from the power spectra. The smallest length-scale values directly characterized in this analysis were defined based on the flow conditions and instrument configuration (sampling frequency and measurement volume). The spatial sampling sizes d_R were computed based in the values of convective velocities of each Cartesian direction and the selected recording frequency. A comparison performed between these values and the size of the sampling volume of the selected acoustic sensor showed that the spatial resolution of the analysis was defined by the sensor geometry of the acoustic beams (diameter = 6 mm) for air discharges $Q_g \leq 0.61$ L/s because d_R was smaller than the

sampling volume. For the other air discharges analyzed, the spatial resolution was larger than the sampling volume but in all the cases smaller than 3 cm.

6.4 Dissipation rate of turbulent kinetic energy

Energy dissipation rate of turbulent kinetic energy ε , was computed from $-5/3$ slope fitting in the inertial range of the observed one-dimensional power spectrum in the spatial domain as $E_{xx}(k_x) = C_x k_x^{-5/3} \varepsilon^{2/3}$, where $C_x = 0.49$ (Pope 2000). The wave number k_x was computed from the frequency f using the Taylor hypothesis as $k_x = 2\pi f/U_c$, where U_c is the convective velocity in the vertical direction x at the point where measurements were taken. Using the same Taylor hypothesis, the one-dimensional spectrum in the spatial domain for the direction x , E_{xx} , was computed from the one dimensional power spectrum G_{xx} , in the frequency domain as

$$E_{xx}(k_x) = \frac{U_c}{2\pi} G_{xx} \left(\frac{k_x U_c}{2\pi} \right). \quad (3)$$

The limits of the range where the fitting was performed were defined as the region where the data had a slope of $-5/3 \pm 15\%$. The power law spectrum used in the fitting assumes an isotropic turbulence. The analyzed velocity time signals correspond to a region in the tank far from the bubble-plume core, water surface, tank walls and bottom, thus the hypothesis of isotropic turbulence should be a good approximation. This assumption is validated comparing longitudinal and lateral power spectrum within the inertial range in order to contrast with the expression for the isotropic turbulence proposed by Pope (2000): $E_{yy}(k_x) = E_{zz}(k_x) = 4/3 E_{xx}(k_x)$. The power spectra used in the comparison were computed through the FFT of the windowed data (a rectangular window was used) and the number of segments (Bendat and Piersol 2000) used to get the average power spectra was maximized (512 samples in each segment) to minimize the uncertainty in the reported values of the power spectra for the inertial range. The observed values of the cited ratios were $E_{xx}(k_x)/E_{yy}(k_x) = 1.27$ and $E_{yy}(k_x)/E_{zz}(k_x) = 0.81$ for the air discharge $Q_g = 16.52$ L/s, which agree reasonably well with the values proposed by Pope (2000).

6.5 Confidence intervals for the turbulence parameters

In order to define trends and to compare the results with reported data available in the literature, an estimation of the errors involved in the computation of each parameter was performed. The error involved in the experimental determination of a turbulence parameter presents several components: errors due to the experimental setup (i.e. misallocation of the instrument);

errors due to the physical constraint of the measurement technique (i.e. size of the sampling volume and sampling frequency of the instrument); statistical errors due to sampling a random signal, and errors due to the methodology used to compute the parameters (e.g. scaling relations provide only orders of magnitude of the parameter). An approximation for the confidence intervals (95% confidence) for each turbulence parameter is computed herein using the moving block bootstrap technique (MBB) that was found by García et al. (2005b) to provide a good approximation for quantifying the statistical errors of the turbulence parameters which generate scatter in repeated measurements of parameters when the same experimental setup, instrument, and methodology are used. A key parameter in the MBB technique is the optimum length of the block. The optimum block length considered here was estimated using the methodology proposed by Politis and White (2004) based on the observed values of the autocorrelation function for each recorded signal (García et al. 2005b).

The estimation of the statistical error by MBB provides a good estimate of the total error when the others errors components are minimized and relatively small compared to the sampling error. Errors due to the experimental setup were minimized during the experiments. The errors due to the physical constraint of the measurement were discussed in Sect. 3. These errors were negligible for the experimental conditions described in this paper. Thus, the statistical errors estimated by using MBB provided a good approximation of the total error for all the turbulence parameters, except for those parameters (i.e. as the Kolmogorov length scale) that are estimated using a scaling relation which provides an order of magnitude estimate of the size of the dissipating eddies. For those parameters, the uncertainty in the selected methodology used in the determination is higher than the statistical errors (reproduced by MBB).

7 Analysis of results

The main results reported here include an analysis of the behavior of the different turbulence parameters and the contribution to them by different turbulence-generating processes as the diffuser air discharge is increased. The analysis was performed on water-velocity signals recorded at a defined location in the tank (radial location: 3.96 m from the axis, vertical location: 2.5 m above the diffuser). The results reported for this location, represent well the average values computed for an intermediate region of the tank ($0.16 \leq r/R \leq 0.71$, where r and R are the radial location from the center of the tank and the radius of the tank, respectively), distant from the plume, water surface, walls and bottom with a homogenous behavior of the turbulence parameters. The observed differences between values of the parameters computed for the selected location and averages in the

analyzed region were of the same order or smaller than the confidence intervals of each parameter.

The evolution with the air discharge of the mean water velocities in the radial and vertical directions is shown in Fig. 7. The mean tangential velocities were negligible (< 0.8 cm/s) at the defined location for all the tested experimental conditions.

Negative mean radial velocities in Fig. 7 imply water flowing back to the center of the tank due to the general recirculation induced by the bubble-plume. At the selected radial location (3.96 m from the center of the tank), the zero radial velocity point is about 4 m above the diffuser; locations upper than 4 m showed positive radial velocity values with water flowing out of the bubble-plume core region. A clear relation between radial velocity component and air discharge is observed in Fig. 7 and a log fit (coefficient of determination equal to 0.96 indicates the goodness of fit) is included as $V_{\text{radial}} = -[2.31 \ln(Q_g) + 2.66]$, (velocities in cm/s and air discharges in L/s). Positive vertical velocities, indicating an upward flow, were observed at the selected location for the whole range of Q_g . The vertical velocities did not show a clear trend for $Q_g > 0.61$ L/s, being a constant value a valid fit for the observed data. The coefficients of variation (CV) of the mean parameter computed through the ratio between the standard deviation of the parameter estimated using MBB and the expected value of the parameter were smaller than 10 and 12% for the mean values of the radial and vertical velocity components, respectively, for $Q_g \geq 0.61$ L/s. Mean velocities values of both components presented large coefficients of variation for Q_g of 0.19 L/s due to the very small value for both velocity components.

Two data sets of turbulent kinetic energy TKE values are shown in Fig. 8: (a) TKE values including fluctuation contributions from all the turbulence process and (b) TKE values including only fluctuation contributions from the intermediate- and micro-scale turbulence

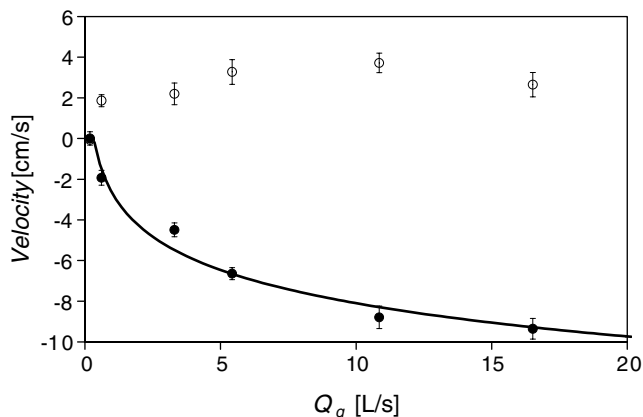


Fig. 7 Evolution with the air discharges Q_g of the mean velocities in the vertical (*open circle*) and radial direction (*filled circle*) at radial location 3.96 m from the axis, 2.5 m above the diffuser. The 95% confidence intervals are included in the plot as well as the log fit for the radial velocity component (*continuous line*)

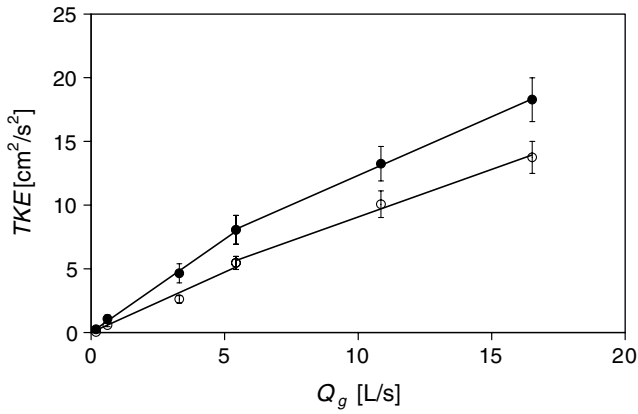


Fig. 8 Evolution of the TKE with the air discharges Q_g at radial location 3.96 m from the axis, 2.5 m above the diffuser. (filled circle) TKE due to fluctuation contributions from all the turbulence process; and (open circle) TKE due to fluctuation contributions from only the intermediate- and micro-scale turbulence process. The difference between the two set of data is TKE due to the macro-scale wandering process. A linear fit to the data (continuous line) and the 95% confidence intervals are included

process (computed by high pass filtering the signal to remove the macro-scale turbulence contribution).

Noise energy contributions were removed to compute both sets of TKE values. Although the noise energy was less or equal to 6% of the total TKE (including contributions from all the turbulence processes) for $Q_g \geq 3.30$ L/s, subtracting the noise energy to compute TKE values was relevant for the two smallest tested air discharges (0.19 and 0.61 L/s) that presented the less energetic conditions. In those conditions, the noise energy was about 20% of the total TKE and comparable in magnitude with the TKE values including only contributions from the intermediate- and micro-scale turbulence process.

The difference between the two sets of data plotted in Fig. 8 indicates the contribution to the TKE from the macro-scale turbulent process (wandering motion of the bubble plume). The ratio of the TKE due to the wandering to the total TKE was 84, 45, 44, 32, 24, and 25 % for the air discharges (0.19, 0.61, 3.30, 5.43, 10.85, and 16.52 L/s, respectively). These values indicated that the contribution by the macro-scale turbulence process dominates the total turbulent kinetic energy (and the mixing process) for low air discharges and that the intermediate- and micro-scale turbulence dominates the total TKE for high air discharges (high energy flows). CV values of the TKE estimates were smaller than 17 and 11% for TKE data sets (a) and (b), respectively, for all the range of tested air discharges (CV values were 11 and 6% for $Q_g \geq 0.61$ L/s).

Changes in the slope of the linear fits are clearly observed for the evolution of both sets of TKE data. The computation of an intrinsic length-scale for the bubble plume D helped to analyze the observed behavior. The length scale D , which expresses a balance between inertia and buoyancy, was used in our laboratory

by Bombardelli (2004) to scale vertical and horizontal distances in bubble-plume flows. The scale was computed as $D = (gQ_0)/(4\pi\alpha^2\omega_b^3)$, where Q_0 is the airflow rate at the diffuser, g is the gravity acceleration, ω_b is the bubble-slip velocity and α is the entrainment coefficient. The airflow rate at the diffuser is related to the air flow rate at atmospheric pressure Q_g , by $Q_0 = Q_g H / (h_a + H)$, where h_a is the atmospheric pressure head equal to 10.2 m. An order of magnitude of the length scale D was computed for all the tests using estimates of $\omega_b = 0.3$ m/s and $\alpha = 0.1$. The bubble slip velocity ω_b is governed by the size of the bubbles r_b . Wüest et al. (1992) approximated this relation based on experimental data as: $\omega_b = 4474r_b^{1.357}$ for $r_b < 0.0007$ m; $\omega_b = 0.23$ for $0.0007 \text{ m} < r_b < 0.005$ m; and $\omega_b = 4.202r_b^{0.54}$ for $r_b > 0.005$ m, where ω_b and r_b units are (m/s) and (m), respectively. The selected value of $\omega_b = 0.30$ m/s approximates the expected value of ω_b for $r_b = 0.01$ m (bubbles radius expected to be present for the analyzed experimental conditions) with a difference smaller than 10%. The entrainment coefficient is defined by plume properties as centerline gas fraction and air discharge. The selected value of $\alpha = 0.10$ was adopted in agreement with α values computed by Fannelop and Sjoen (1980) based on data recorded in a laboratory facility having a width of 10.5 m and a depth of 10 m. The α values increased with increased air discharge, being 0.075 for $Q_g = 5$ normal L/s and increasing to 0.012 for a gas flow rate of 22 normal L/s.

For $Q_g = 4$ L/s, D is of the order of the tank radius and this condition agrees with the condition where a change in the TKE behavior was detected for both curves in Fig. 8. For air discharges that generate intrinsic length scales D smaller than the tank radius, steeper slopes of the TKE linear fit were detected for both sets of data.

Figure 9 shows the evolution with the air discharge of the resultant integral length scale L characterizing both

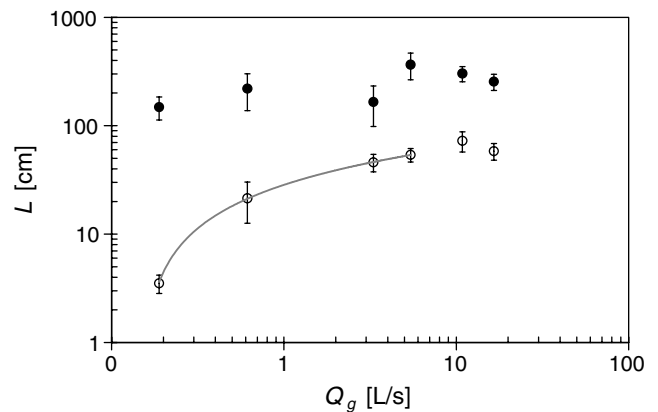


Fig. 9 Evolution with the air discharges of the resultant integral length scale L at radial location 3.96 m from the axis, 2.5 m above the diffuser. (filled circle) L representing all the turbulence process; and (open circle) L representing only the intermediate- and micro-scale turbulence process. A logarithmic fit of the data (continuous line) and the 95% confidence intervals are included

(a) all turbulence processes and (b) only the intermediate- and micro-scale turbulence process. The undesired effects of the digital filtering (used to separate the turbulence process) on the L computation characterizing only the intermediate- and micro-scale turbulence process were discarded because a time scale of the high pass filter equal to 120 s (computed as the inverse of the cut-off frequency f_c of the high pass filter) was used for all the recorded signals, that is much longer than the longest observed integral time scale representing intermediate- and micro-turbulence process at the selected location for all the Cartesian components (6.5 s). The CV values of the resultant turbulence integral length scale parameter were smaller than 21% for all the analyzed air discharges for both data sets. The resultant integral length scale values representing all the turbulence process (dominated by the presence of plume wandering) did not show a clear trend as the air discharge increased and they ranged from 1.49 to 3.66 m, about one order of magnitude larger than the scales representing the intermediate and micro-scale process. The resultant length scale for the intermediate- and micro-scale turbulence process showed a clear trend for air discharges smaller than 5.43 L/s. A logarithmic fit (coefficient of determination equal to 0.9999) of the data was obtained in this range as $L = 14.91 \ln(Q_g) + 28.46$ (L in cm and Q_g in L/s) is included in Fig. 9. For air discharges equal or higher than 5.43 L/s, the resultant length scale gets a constant value (average = 61.5 cm) which is about 10% of the tank radius. The use of the D is relevant in the analysis of the cited behavior. As mentioned previously, D is of the order of the radius of the tank for $Q_g = 4$ L/s. The presence of constant values of the L characterizing the intermediate- and micro-scale turbulence process for higher air discharges (D values larger than the radius of the tank) indicated that the tank walls limited the size of the large turbulent structures.

Values of dissipation rate of turbulent kinetic energy ε computed using the $-5/3$ fit in the inertial range of the power spectra obtained from the high pass filtered signal (including only the intermediate- and micro-scale turbulence process) are presented in Fig. 10. The ε values increased as the air discharge increased according to a power-law (coefficient of determination equal to 0.9896) given by $\varepsilon = 0.0116 Q_g^{1.426}$, where ε and Q_g units are (cm^2/s^3) and (L/s), respectively. The CV values of the ε parameter were smaller than 18% for $Q_g > 0.61$ L/s and 32% for $Q_g \leq 0.61$ L/s. Ranges of wave number k_x longer than one order of magnitude within the inertial range were used to perform the $-5/3$ fitting for air discharges $Q_g \geq 0.61$ L/s. An equivalent set of data was computed fitting the $-5/3$ law to the power spectra of signals including all the turbulence processes but the ε estimates were not significantly different (they were within the confidence interval of the values plotted in Fig. 10). A clear change in the behavior of the ε parameter as the air discharge increases was not observed (as it was noticed for TKE and L values) because the geometry of the tank does not affect the micro-scale

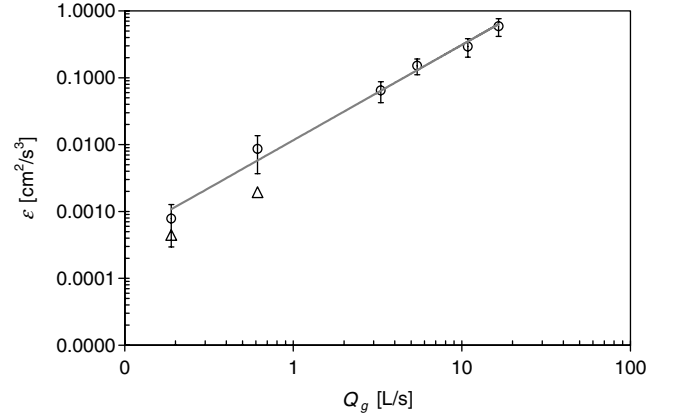


Fig. 10 Evolution with the air discharges of the dissipation rate of turbulent kinetic energy at radial location 3.96 m from the axis, 2.5 m above the diffuser. (open circle) ε computed fitting $-5/3$ law to the power spectra. (open triangle) values computed by Soga and Rehmann (2004) in the same facility using a different instrument (SCAMP). A power-law fit of the data is included as well as the 95% confidence intervals.

turbulence process responsible for the dissipation of TKE. The values of dissipation rate of TKE obtained by Soga and Rehmann (2004) in the same facility using a different measurement technique are also included in Fig. 10. The observations by Soga and Rehmann (2004) were restricted to only the smaller air discharges analyzed here (0.19 and 0.61 L/s) due to SCAMP range of operation (Kocsis et al. 1999). The value of ε observed by Soga and Rehmann (2004) for the smallest Q_g lies within the confidence interval of the ε values reported here for the same air discharge. However, the largest difference was observed for $Q_g = 0.61$ L/s.

Finally, the values of dissipation rate of turbulent kinetic energy plotted in Fig. 10 were used to estimate the order of magnitude of the smallest scale of turbulent motion (Kolmogorov length scale). Figure 11 shows that the Kolmogorov length scale decreases as the air discharge increases according to a power law (coefficient

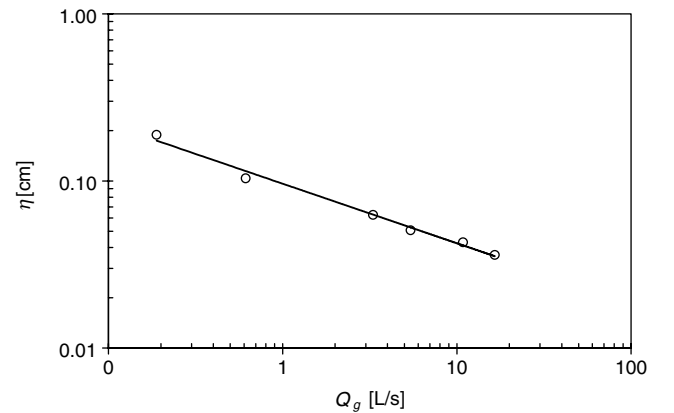


Fig. 11 Evolution with the air discharges of the Kolmogorov length scale at radial location 3.96 m from the axis, 2.5 m above the diffuser. Continuous line a power fit

of determination equal to 0.9896) given by $\eta = 0.0963Q_g^{-0.356}$ where η and Q_g units are (cm) and (L/s). The CV values computed by MBB method are not reported in Fig. 11 because the scaling relation used in the estimation of η yields an order of magnitude of the dissipating eddy sizes. The Kolmogorov scales estimated herein were smaller than the smallest possible size of the spatial resolution (the size of the sampling volume = 0.6 cm) for all the air discharges, but they can be still considered valid because they were obtained indirectly from scaling (not directly from visual inspection of the observed power spectrum).

8 Summary and conclusions

Flow turbulence generated by a bubble plume in a large tank at a wastewater-treatment plant was characterized. The acoustic Doppler velocimetry technique was used to record water-velocity signals in the large facility (outside of the bubble-plume core) because it provided a good description of the flow turbulence in adverse experimental conditions that included the use of raw sewage influents. The achieved time and spatial resolution for the turbulence characterization in the large facility was comparable to resolutions obtained by other laboratory measurement techniques in much smaller facilities.

Two main different turbulence processes were identified with the help of water-velocity signals recorded outside of the bubble-plume core: (a) a macro-scale turbulence process (wandering motion of the bubble plume) which was clearly observed through a peak at the low frequency component of the computed power spectrum; and (b) the intermediate- and micro-scale turbulence process that was well represented by the Kolmogorov power spectrum. Both turbulence processes contribute in a different way to the mixing and transport process in the tank. A methodology was presented to characterize the different turbulent scales generated by a bubble-plume in a large tank and their contributions to the turbulence parameters. Wandering periods computed for the different experimental conditions were about two orders of magnitude longer than the integral time scale of the intermediate- and micro-scale turbulence process. This result allowed for the use of a separation technique (high pass filtering) to obtain information characterizing each turbulence process. The main results presented in this paper consist of an analysis of the behavior of different turbulence parameters and the contribution to them of the different turbulence process as the air discharge Q_g increased at a fixed location in the tank. This location was selected to represent an intermediate region of the tank distant from the plume, water surface, walls, and bottom with a homogenous behavior of the parameters.

The relative contribution of the macro-scale turbulence process (wandering) to the total turbulent kinetic energy TKE at the defined location decreased from 84 to 25% as Q_g increased from 0.19 to 16.52 L/s. This result

indicated that the macro-scale turbulence process dominated the total TKE (and the mixing process) for the smaller tested Q_g and the micro- and intermediate-scale turbulence did for the highest Q_g . The resultant integral length scales L representing all the turbulence processes (dominated by the presence of plume wandering) were about one order of magnitude larger than the scales representing the intermediate- and micro-scale process. Significant changes were observed in the behaviors of TKE and L parameters as Q_g increased. An intrinsic length scale of the bubble plume D expressing a balance between inertia and buoyancy was used to explain these behaviors. It was found that the change in behavior agreed with the point where the length scale D of the bubble plume was of the order of the tank radius. The resultant integral length scale for the intermediate- and micro-scale turbulence process showed a clear increasing log trend for flow conditions presenting D values smaller than the tank radius. For flow conditions with D larger than the radius of the tank, the resultant length scale obtained a constant value of about 10% of the tank radius. The reason for L reaching a constant value is because the tank walls limited the size of the large micro- and intermediate-turbulence structures. Regarding to the TKE values, flow conditions with D smaller than the tank radius, presented steep slopes on the linear fit of TKE values. No significant change was observed in the behavior of the parameters dissipation rate of TKE and Kolmogorov length scale as the air discharge and the length scale D increased. The results summarized here provide a basis for the validation of numerical models of bubble-plume systems used in the design of combined-sewer-overflow reservoirs. They can also be used to conduct a preliminary design of coarse-bubble diffuser for reservoir mixing.

Acknowledgments The financial support of the U.S. Army Corps of Engineers, Chicago District, is acknowledged. The support by the U.S. Geological Survey (Office of Surface Water) and the Metropolitan Water Reclamation District of Greater Chicago during the data-analysis stage of this work are also acknowledged. The opinions and findings presented here are solely those of the authors. We acknowledge the help of A. Waratuke, F. Bombardelli, M. Cantero, G. Johnson and L. Rincon, preparing the experimental facility and conducting the experiments. The experiments would not have been possible without the access to the digester tank provided by the Urbana and Champaign Sanitary District.

References

- Baines W, Hamilton G (1959) On the flow of water induced by a rising column of air bubbles. IAHR. In: Proceedings of 8th Congress. Montreal (2):7D1–7D11
- Becker S, Sokolichin A, Eigenberger G (1994) Gas–liquid flow in bubble columns and loop reactors: Part II. Comparison of detailed experiments and flow simulations. Chem Eng Sci 24B:5747–5762
- Becker S, De Bie H, Sweeney J (1999) Dynamic flow behaviour in bubble columns. Chem Eng Sci 54:4929–4935
- Bendat J, Piersol A (2000) Random data, 3rd edn. Wiley, New York

- Bombardelli F (2004) Turbulence in multiphase models for aeration bubble plumes. PhD thesis. University of Illinois at Urbana-Champaign. Urbana, Illinois
- Buwa V, Ranade V (2002) Dynamics of gas-liquid flow in a rectangular bubble column: experiments and single/multi-group CFD simulations. *Chem Eng Sci* 57:4715–4736
- Delnoij E, Kuipers J, Van Swaaij W (1997) Dynamic simulation of gas-liquid two-phase flow: effect of column aspect ratio on the flow structure. *Chem Eng Sci* 52:3759–3772
- Fannelop T, Sjoen K (1980) Hydrodynamics of underwater blow-outs. AIAA 8th Aerospace Sciences Meeting, January 14–16, AIAA paper, 80 pp. Pasadena, California
- Fannelop T, Hirschberg S, Kuffer J (1991) Surface current and recirculating cells generated by bubble curtains and jets. *J Fluid Mech* 229:629–657
- Fischer J, Kumazawa H, Sada E (1994) On the local gas holdup and flow pattern in standard-type bubble columns. *Chem Eng Process* 33:7–21
- García C, Cantero M, Niño Y, García M (2005a) Turbulence measurements with acoustic Doppler velocimeters. *J Hydraul Eng ASCE* 131:1062–1073
- García C, Jackson P, García M (2005b) Confidence intervals in the determination of turbulence parameter. *Exp Fluids*. DOI: 10.1007/s00348-005-0091-8
- Heskestad G (1965) A generalized Taylor Hypothesis with application for high Reynolds number turbulent shear flows. *J Appl Mech* 32:735–739
- Johansen S, Robertson D, Woje K, Engh T (1988) Fluid dynamics in bubble stirred ladles: Part I. Experiments. *Metall Trans B* 19B:745–754
- Johnson G, Hornewer N, Robertson D, Olson D, Gioja J (2000) Methodology, data collection, and data analysis for determination of water-mixing patterns induced by aerators and mixers. Water Resources Investigation Report 00-4101. U.S. Geological Survey
- Joshi J, Vitankar V, Kulkarni A, Dhotre M, Ekambara K (2002) Coherent flow structures in bubble column reactors. *Chem Eng Sci* 57:3157–3183
- Kobus H (1968) Analysis of the flow induced by air-bubble systems. In: Proceedings of Coastal Engineering Conference. London, II, pp 1016–10312
- Kocsis O, Prandke H, Stips A, Simon A, Wüest A (1999) Comparison of dissipation of turbulent kinetic energy determined from shear and temperature microstructure. *J Mar Syst* 21: 67–84
- Kresta S, Wood P (1993) The flow field produced by a pitched blade turbine. Characterization of the turbulence and estimation of the dissipation rate. *Chem Eng Sci* 48:1761–1774
- Lohrmann A, Cabrera R, Kraus N (1994) Acoustic Doppler velocimeter (ADV) for laboratory use. In: Proceedings from Symposium on fundamentals and Advancements in Hydraulic measurements and Experimentation, ASCE. Buffalo 351–365
- Milgram J (1983) Mean flow in round bubble plumes. *J Fluid Mech* 133:345–376
- Mudde R (2005) Gravity-driven bubbly flows. *Annu Rev Fluid Mech* 37:393–423
- Mudde R, Groen J, Van Den Akker H (1997a) Liquid velocity field in a bubble column: LDA experiments. *Chem Eng Sci* 52:4217–4224
- Mudde R, Lee D, Reese J, Fan L (1997b) Role of coherent structures on Reynolds stresses in a 2-D bubble column. *AIChE J* 43:913–926
- Nikora V, Goring D (1998) ADV measurements of turbulence: can we improve their interpretation? *J Hydraul Eng ASCE* 124:630–634
- Politis D, White H (2004) Automatic block-length selection for the dependant bootstrap. *Econ Rev* 23:53–70
- Pope S (2000) Turbulent flows. Cambridge, UK
- Rensen J, Roig V (2001) Experimental study of the unsteady structure of a confined bubble plume. *Int J Multiph Flow* 27:1431–1449
- Soga C, Rehmann C (2004) Dissipation of turbulent kinetic energy near a bubble plume. *J Hydraul Eng* 130:441–449
- Tekeli S, Maxwell W (1978) Behavior of air bubble screens. Civil Engineering studies, Hydraulic Research series No 33. University of Illinois at Urbana, Champaign
- Voulgaris G, Trowbridge J (1998) Evaluation of the acoustic Doppler velocimeter (ADV) for turbulence measurements. *J Atmos Ocean Technol* 15:272–288
- Wain D, Rehmann C (2005) Eddy diffusivity near bubble plumes. *Water Resour Res* 41:W09409
- Wernersson E, Trägårdh C (2000) Measurements and analysis of high-intensity turbulent characteristics in a turbine-agitated tank. *Exp Fluids* 28:532–545
- Wu H, Patterson G (1989) Laser-Doppler measurements of turbulent-flow parameters in a stirred mixer. *Chem Eng Sci* 44:2207–2221
- Wüest A, Brooks N, Imboden D (1992) Bubble plume modeling for Lake restoration. *Water Resour Res* 28:3235–3250